Journal of Alloys and Compounds 720 (2017) 277–283

Contents lists available at ScienceDirect

Journal of Alloys and Compounds

journal homepage: http://www.elsevier.com/locate/jalcom

Hydrogen dynamics in the hexagonal $Ho_2Fe_{17}H_4$ and $Y_2Fe_{17}H_{4.2}$: Inelastic and quasielastic neutron scattering studies

A.V. Skripov [a, *], O. Isnard [b, c], N.V. Mushnikov [a, d], P.B. Terent'ev [a, d], V.S. Gaviko [a, d], T.J. Udovic [e]

[a] Institute of Metal Physics, Ural Branch of the Russian Academy of Sciences, Ekaterinburg 620990, Russia
[b] CNRS, Institut Néel, CNRS, BP 166X, F-38042 Grenoble, France
[c] Université Grenoble Alpes, Institut Néel, F-38042 Grenoble, France
[d] Yeltsin Ural Federal University, Ekaterinburg 620002, Russia
[e] NIST Center for Neutron Research, National Institute of Standards and Technology, Gaithersburg, MD 20899-6102, USA

ARTICLE INFO

Article history:
Received 28 March 2017
Received in revised form
26 May 2017
Accepted 27 May 2017
Available online 28 May 2017

Keywords:
Metal hydrides
Diffusion
Inelastic neutron scattering

ABSTRACT

The vibrational spectra of hydrogen and the parameters of H jump motion in the hexagonal Th_2Ni_{17}-type compounds $Ho_2Fe_{17}H_4$ and $Y_2Fe_{17}H_{4.2}$ have been studied by means of inelastic and quasielastic neutron scattering. It is found that hydrogen atoms occupying interstitial $Ho(Y)_2Fe_2$ sites in both compounds participate in the fast localized jump motion over the hexagons formed by these tetrahedral sites. The temperature dependence of the H jump rate is well described by the Arrhenius law over wide T ranges (100–340 K for $Ho_2Fe_{17}H_4$ and 140–360 K for $Y_2Fe_{17}H_{4.2}$) with the activation energies of 54 (4) meV and 84 (7) meV, respectively. For $Ho_2Fe_{17}H_4$, the localized hydrogen jump motion is found to be the fastest among all R_2Fe_{17} hydrides studied so far. At room temperature, the H jump rate in $Ho_2Fe_{17}H_4$ derived from our quasielastic neutron scattering data reaches 6.4×10^{11} s^{-1}.

1. Introduction

Intermetallic compounds R_2Fe_{17} (where R is yttrium or rare-earth element) are known to adopt either the rhombohedral Th_2Zn_{17}-type or the hexagonal Th_2Ni_{17}-type structure. Owing to their interesting magnetic properties, these compounds have been extensively studied since the late sixties [1–5]. The renewed interest to the R_2Fe_{17} intermetallics is related to the discovery of dramatic changes in their magnetic properties upon hydrogen uptake [6–8]. In particular, hydrogenation of the R_2Fe_{17} compounds leads to a strong increase in the Curie temperature and magnetization [6–12], which makes these materials attractive candidates for permanent magnet applications. The structural aspects of hydrogenated $R_2Fe_{17}H_x$ compounds have been summarized by Isnard et al. [6,8,11]. For materials of both structural types, the host lattice retains its structure after hydrogenation, showing anisotropic expansion with increasing H content. Initially, H atoms fill the distorted octahedral (o) interstitial sites formed by four Fe atoms and two R atoms, and at $x = 3$, these sites are fully occupied. Further hydrogenation leads to a partial filling of the tetrahedral (t) interstitial sites coordinated by two Fe and two R atoms. In materials of both structural types, the sublattice of these tetrahedral sites consists of regular hexagons in the basal plane with a side dimension of ~1.1–1.2 Å. Because of the repulsive interaction between hydrogen atoms in metals, H atoms cannot simultaneously occupy the sites separated by the distances of ~2.1 Å or less (the "blocking" effect) [13]. Therefore, each t-site hexagon can accommodate up to two H atoms, so that the maximum occupancy of t sites is 1/3. The maximum H content in $R_2Fe_{17}H_x$ is $x = 5$, which corresponds to the complete filling of o sites and a one-third filling of t sites. Experimentally, this maximum H content was attained for the rhombohedral Th_2Zn_{17}-type hydrides, while for the hexagonal Th_2Ni_{17}-type hydrides the maximum attainable value of x remains lower than 5 and decreases along with the lanthanide contraction. It has been shown by both *in situ* neutron diffraction and differential scanning calorimetry investigations that the octahedral sites are more stable than the tetrahedral ones [14,15], the hydrogen desorption occurring first for the smaller tetrahedral positions.

The peculiar sublattice of partially occupied interstitial sites in $R_2Fe_{17}H_x$ may be responsible for unusual hydrogen dynamics in these compounds. Since the t-site hexagons are well separated

* Corresponding author.
E-mail address: skripov@imp.uran.ru (A.V. Skripov).

http://dx.doi.org/10.1016/j.jallcom.2017.05.300
0925-8388/

from each other and from *o* sites, one may expect a localized motion of H atoms over these hexagons. The existence of fast H jump motion in the rhombohedral $Pr_2Fe_{17}H_x$ was first revealed by Mössbauer spectroscopy [16]. Subsequent quasielastic neutron scattering (QENS) experiments in Th_2Zn_{17}-type $Pr_2Fe_{17}H_x$ [17,18] and $Ce_2Fe_{17}H_5$ [19] gave the direct evidence that this fast jump process corresponds to localized H motion over the *t*-site hexagons. The most intriguing feature of the QENS results [17–19] is that the localized H motion is not suppressed by the repulsive H–H interaction due to the presence of two hydrogen atoms at each hexagon. Thus, the jump motion of two H atoms occupying the opposite vertices of the same hexagon should be correlated, as if these atoms formed a bound pair. In the hexagonal Th_2Ni_{17}-type compounds, hydrogen dynamics has not been studied thus far. The aim of the present work is to investigate both the vibrational spectrum of hydrogen and the jump motion of H atoms in the hexagonal Th_2Ni_{17}-type compounds Ho_2Fe_{17} and Y_2Fe_{17} using inelastic and quasielastic neutron scattering measurements. The results will be compared to those obtained for the rhombohedral Th_2Zn_{17}-type compounds. We shall also discuss the effects of changes in dimensions of the *t*-site hexagons and in occupancy of these hexagons on the parameters of H jump motion in the R_2Fe_{17} intermetallics.

2. Experimental details

Intermetallic compounds Ho_2Fe_{17} and Y_2Fe_{17} were prepared by arc melting in an argon atmosphere followed by annealing in argon at 1273 K for 72 h. According to X-ray diffraction analysis, the annealed sample of Ho_2Fe_{17} was a single-phase compound with the hexagonal Th_2Ni_{17}-type structure (space group $P6_3/mmc$) and the lattice parameters $a = 8.451$ Å and $c = 8.292$ Å. For the annealed Y_2Fe_{17} sample, the dominant phase also had the hexagonal Th_2Ni_{17}-type structure with $a = 8.464$ Å and $c = 8.362$ Å; this sample contained traces of residual α-Fe. Both samples were hydrogenated in a Sieverts-type apparatus using $LaNi_5$ hydride as a source of pure hydrogen at a temperature of 488 K and a hydrogen pressure of 15 bar. The host lattice of both hydrogenated samples was found to retain the Th_2Ni_{17}-type structure with the increased lattice parameters: $a = 8.547$ Å and $c = 8.341$ Å for $Ho_2Fe_{17}H_x$, and $a = 8.565$ Å and $c = 8.362$ Å for the dominant phase of $Y_2Fe_{17}H_x$. The lattice parameters of the residual α-Fe phase did not change after hydrogenation; this means that α-Fe does not absorb hydrogen under the present conditions. The hydrogen content per formula unit, *x*, estimated gravimetrically was 4.0 (1) H atoms per formula unit for $Ho_2Fe_{17}H_x$ and 4.2 (1) H atoms per formula unit for $Y_2Fe_{17}H_x$. Note that the lattice parameters of $Ho_2Fe_{17}H_4$ and $Y_2Fe_{17}H_{4.2}$ are consistent with the corresponding previous results on the hydrides with similar compositions [6,8].

All neutron scattering experiments were performed at the NIST Center for Neutron Research (Gaithersburg, Maryland, USA). The inelastic neutron scattering measurements of the hydrogen vibrational spectra at 4 K were made on a filter-analyzer neutron spectrometer (FANS) [20] using the Cu(220) monochromator and horizontal collimation of 20 min of arc before and after the monochromator. The measured range of neutron energy loss was 40–160 meV, and the energy resolution was about 3% of the energy transfer. Measurements of QENS spectra $S_{exp}(Q,\omega)$ (where $\hbar\omega$ is the energy transfer and $\hbar Q$ is the elastic momentum transfer) were performed on the time-of-flight disk-chopper spectrometer (DCS) [21] and the high-flux backscattering spectrometer (HFBS) [22] using the incident neutron wavelengths λ of 6.0 Å (DCS) and 6.27 Å (HFBS). These two spectrometers complement each other with respect to the energy resolution and the accessible range of energy transfer. In our experiments, the energy resolution full widths at half-maximum (FWHM) were 67 μeV (DCS) and 1.0 μeV (HFBS). The ranges of the elastic momentum transfer studied corresponded to *Q* ranges of 0.39–1.70 $Å^{-1}$ (DCS) and 0.25–1.75 $Å^{-1}$ (HFBS). The powdered $Ho_2Fe_{17}H_4$ and $Y_2Fe_{17}H_{4.2}$ samples were studied in annular geometry in a hollow-cylinder Al container, the sample thickness being about 0.3 mm. The sample thickness was chosen to ensure ~90% neutron transmission and thus minimize multiple-scattering effects. For analysis of the DCS data, the detectors were binned into eight groups. The scattering angles corresponding to the Bragg reflections were excluded from the analysis. The instrumental resolution functions $R(Q, \omega)$ were determined from the measured QENS spectra for $Ho_2Fe_{17}H_4$ and $Y_2Fe_{17}H_{4.2}$ at low temperatures (25 K for DCS and 4 K for HFBS).

It should be noted that statistical uncertainties in all figures, if not explicitly indicated by error bars, are commensurate with the observed scatter in the data.

3. Results and discussion

3.1. Neutron vibrational spectroscopy

A schematic view of the hexagonal Th_2Ni_{17}-type structure of $Ho_2Fe_{17}H_x$ with the octahedral (6*h*) and tetrahedral (12*i*) hydrogen sites is shown in Fig. 1(a). Fig. 1(b) represents a hexagon formed by the tetrahedral 12*i* sites in the basal plane. The experimental low-temperature INS spectra for $Ho_2Fe_{17}H_4$ and $Y_2Fe_{17}H_{4.2}$ are shown in Figs. 2 and 3, respectively. The H incoherent neutron scattering cross section overwhelmingly dominates those for Ho, Y, and Fe, so that the INS spectrum from a filter-analyzer-type spectrometer, such as FANS, approximates the H vibrational density of states (VDOS) averaged over *Q* space [20]. As can be seen from Figs. 2 and 3, INS spectra for both compounds have similar shapes in the studied energy transfer range. The strongest peak in the spectrum is observed near 85 meV for $Ho_2Fe_{17}H_4$ and near 87 meV for $Y_2Fe_{17}H_{4.2}$. At higher energy transfers, there are additional scattering features between 90 and 130 meV. For metal – hydrogen systems, low-temperature INS spectra in the energy transfer range 40–160 meV are usually dominated by the fundamental modes of H optical vibrations. The simplest approach to the description of these vibrations is based on the model of a three-dimensional Einstein oscillator [23,24]. For the $\hbar\omega$ range of fundamental modes, this model predicts three peaks of nearly equal intensity. Depending on the point symmetry of H sites, all or two of these peaks may be degenerate. For hydrogen in both 6*h* and 12*i* sites of the Th_2Ni_{17}-type compounds, the local symmetry is lower than axial; therefore we may generally expect three peaks for hydrogen in each of these sites. Although this simple Einstein oscillator model might be sufficient for description of an isolated interstitial H atom in a metallic lattice, in reality, hydrides are often far from dilute. Hence, significant interactions between neighboring and even more distant H atoms often result in noticeable dispersion in the measured VDOS. Indeed, in the more extensive prior INS studies of $Pr_2Fe_{17}H_x$ and their deuterated analogues [25], there was clear evidence of phonon dispersion due to various H–H interactions as well as additional overlapping yet minor contributions from broad combination bands involving low-energy (~14 meV) acoustic modes and the fundamental optical-mode transitions. Nonetheless, by measuring multiple spectra as functions of H and D concentrations, the various H normal-mode vibrations could be assigned, and a significant anisotropy was deduced for the potential wells associated with H atoms in the interstitial *t* sites [25]. For the present hexagonal hydrides, all the observed peaks are considerably broader than the instrumental resolution (see Figs. 2 and 3); therefore, phonon dispersion effects should also be significant for $Ho_2Fe_{17}H_4$ and $Y_2Fe_{17}H_{4.2}$. Even though the range of INS data for the

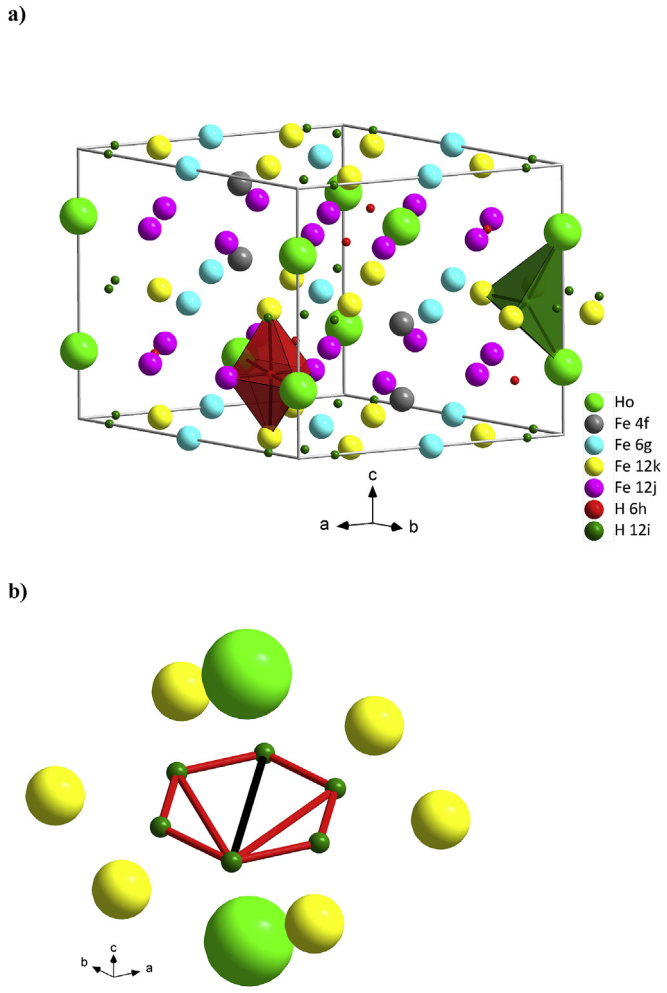

Fig. 1. a) Schematic view of the hexagonal Th_2Ni_{17}-type structure (space group $P6_3/mmc$) of $Ho_2Fe_{17}H_x$ with the octahedral (6*h*) and tetrahedral (12*i*) hydrogen sites. **b)** A hexagon formed by the tetrahedral 12*i* sites in the basal plane. The black line connects the sites which can be simultaneously occupied by H atoms (the intersite distance is ~2.34 Å); the red lines connect the sites which cannot be simultaneously occupied by H atoms due to the "blocking" effect (the intersite distances are less than 2.1 Å). (For interpretation of the references to colour in this figure legend, the reader is referred to the web version of this article.)

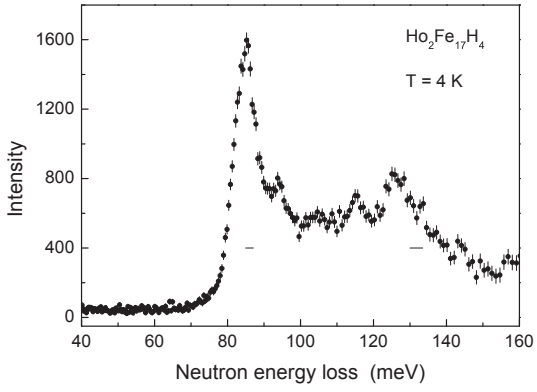

Fig. 2. The low-temperature inelastic neutron scattering spectrum for $Ho_2Fe_{17}H_4$. The horizontal bars indicate the instrumental resolution FWHM in two parts of the spectrum.

present hexagonal hydrides is much more limited than for $Pr_2Fe_{17}H_x$ (i.e., only being measured for single hydrogen

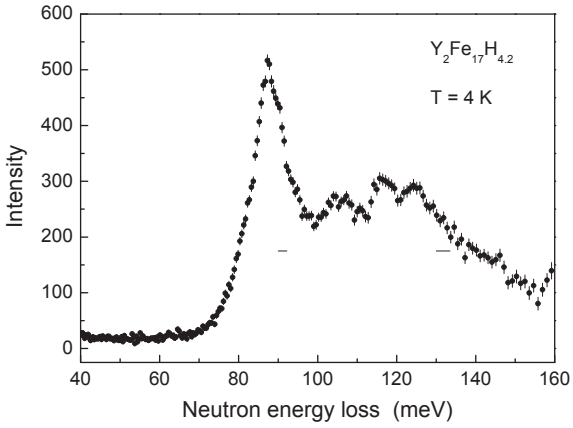

Fig. 3. The low-temperature inelastic neutron scattering spectrum for $Y_2Fe_{17}H_{4.2}$. The horizontal bars indicate the instrumental resolution FWHM in two parts of the spectrum.

concentrations), and the spectra are clouded by phonon dispersion effects and opto-acoustic combination-band scattering, we can still establish reasonable assignments for some fundamental vibrational features based on geometric site arguments and the previous analyses for $Pr_2Fe_{17}H_x$ [25] and $Ce_2Fe_{17}H_5$ [19].

The preference for forming either the hexagonal Th_2Ni_{17}-type or rhombohedral Th_2Zn_{17}-type structure is directly influenced by the relative size of the *R* element [6], with Ho and Y favoring the former structure, and the slightly larger elements (by 3–5% [26]) Pr and Ce the latter. Even though both structures possess R_2Fe_2 tetrahedral sites and R_2Fe_4 octahedral sites (with *R* atoms at opposite apical positions) amenable to H absorption, there are some notable differences in the site aspect ratios between structure types. For example, for the Pr_2Fe_4 *o* sites in rhombohedral $Pr_2Fe_{17}H_x$, the Pr–Pr distance is about 5.02 Å, and the Pr–H–Pr directed bonding within the basal plane thus exhibits about a 0.25 Å shorter Pr–H bond distance (2.51 Å [27]) than seen for *o*-site H in cubic close-packed (ccp) PrH_{2+x} (~2.76 Å [28]). As a result, the H vibrational energy along the Pr–H–Pr axis in $Pr_2Fe_{17}H_x$ was found to be near 106 meV [25], up to around 30 meV higher than for *o*-site H in PrH_{2+x} [29]. In comparison, for hexagonal $Y_2Fe_{17}H_{4.2}$ (and with similar distance arguments for $Ho_2Fe_{17}H_4$), the *o*-site Y–Y distance is 4.94 Å, yielding the Y–H bond distance of ~2.47 Å [8], which is only ~0.13 Å shorter than seen for *o*-site H in ccp YH_{2+x} (~2.60 Å [30]). Hence, one would expect vibrational energies slightly higher than the 80 meV *o*-site vibrational energy observed for YH_{2+x} [29], and it is likely that the large respective features at 85 and 87 meV in Figs. 2 and 3 for $Ho_2Fe_{17}H_4$ and $Y_2Fe_{17}H_{4.2}$ indeed reflect, in part, these *R*-H-*R*-directed *o*-site H vibrations. The dominant intensities of these features indicate that another of the *o*-site normal modes is also contributing with similar energies, namely, H vibrations along the *c*-oriented Fe–H–Fe axis with a ~2.0–2.1 Å Fe–H bond distance for both hexagonal R_2Fe_{17} hydrides [6,8]. This is consistent with the 85 meV analogous *c*-oriented Fe–H–Fe vibrations (with a ~1.99 Å Fe–H bond distance) observed in $Pr_2Fe_{17}H_x$ [25].

Another notable difference between the *o* sites for the two structure types involves the remaining H vibration along the orthogonal basal-plane-directed Fe–H–Fe axis. For rhombohedral $Pr_2Fe_{17}H_x$, the Fe–H bond distance in this direction is ~1.89 Å, yielding the H vibrational energy near 106 meV, similar to the bond distance observed for *o*-site H in dhcp Fe hydride [31], with the corresponding vibrational energy of 105 meV [32]. In contrast, the corresponding basal-plane Fe–H distances in the hexagonal R_2Fe_{17} hydrides are much shorter (1.68–1.78 Å [6,8]), which strongly suggests that the respective mode energy is significantly above

106 meV, possibly even associated with the highest modes observed near 125 meV in Figs. 2 and 3. A more definite assignment of this third *o*-site mode would greatly benefit from measuring INS spectra for these hydrides with $x \leq 3$ (i.e., with only *o*-site occupations).

Besides this high-energy *o*-site mode, much of the multi-peak structure in the range of 90–130 meV in Figs. 2 and 3 can be attributed to the three orthogonal H vibrations in the tetrahedral 12*i* sites. Such an assignment is reasonable and consistent with the smaller size of the *t* sites, as compared to the *o* sites. Although it is clear that the *t*-site H vibrations are reflected in these higher-energy scattering features, more detailed assignments would require additional INS measurements at different H (and D) concentrations.

3.2. Quasielastic neutron scattering

Because of the very large incoherent scattering cross-section of hydrogen, the observed neutron scattering from our samples is dominated by the incoherent nuclear scattering on protons. The relative contributions of the host-metal nuclei estimated on the basis of their incoherent scattering cross-sections are 2.3% for $Ho_2Fe_{17}H_4$ and 2.1% for $Y_2Fe_{17}H_{4.2}$. At $T = 25$ K, the H jump motion is "frozen" at the time scale determined by the energy resolution of the time-of-flight neutron spectrometer DCS. The experimental QENS spectra measured on DCS at 25 K have been used to obtain the corresponding instrumental resolution functions $R(Q, \omega)$. At higher temperatures (220–340 K for $Ho_2Fe_{17}H_4$ and 250–360 K for $Y_2Fe_{17}H_{4.2}$), the observed time-of-flight QENS spectra can be satisfactorily described by a sum of two components: an 'elastic' line represented by the DCS resolution function and a resolution-broadened Lorentzian 'quasielastic' line. The relative intensity of the 'quasielastic' component is found to increase with increasing Q, its half-width being nearly Q-independent. These features are typical of the case of spatially-restricted (localized) atomic motion [33,34]. The experimental scattering function $S_{exp}(Q, \omega)$ has been fitted with the model incoherent scattering function,

$$S_{inc}(Q, \omega) = A_0(Q)\delta(\omega) + A_1(Q)L(\omega, \Gamma) \quad (1)$$

convoluted with $R(Q, \omega)$. Here, $\delta(\omega)$ is the elastic δ-function, $L(\omega, \Gamma)$ is the Lorentzian function with the half-width Γ, and $A_0 + A_1 = 1$. As an example of the data, Fig. 4 shows the time-of-flight QENS spectra of $Ho_2Fe_{17}H_4$ recorded at two temperatures (220 and 340 K) and $Q = 1.52$ Å^{-1}. The curves represent the fits of each spectrum with the sum of the 'elastic' and 'quasielastic' components. The width of the 'quasielastic' line is proportional to the H jump rate [33,34]; therefore, the observed significant increase of this width with increasing temperature (Fig. 4) reflects the acceleration of the hydrogen jump motion.

QENS measurements using the backscattering neutron spectrometer HFBS can probe much slower H jump motion than those using the time-of-flight spectrometer DCS. Therefore, HFBS measurements can be used to trace the jump motion at lower temperatures. However, the backscattering QENS measurements are characterized by a rather narrow energy transfer range; this makes them effective only in a limited temperature range. In order to reveal the temperature range where the backscattering QENS measurements could be effective, it is often useful to employ the fixed-window operation mode of the backscattering spectrometer [35]. Fig. 5 shows the temperature dependences of the elastic scattering intensity for $Ho_2Fe_{17}H_4$ and $Y_2Fe_{17}H_{4.2}$ measured over the Q range of 0.87–1.68 Å^{-1} using the fixed-window mode of HFBS. As can be seen from Fig. 5, there is a significant difference between the results of the elastic scans for the two compounds. For $Y_2Fe_{17}H_{4.2}$, the elastic scan exhibits a characteristic step in the range 130–170 K. In this range, one can expect the most pronounced quasielastic line broadening due to the onset of H jump motion on the time scale corresponding to the HFBS resolution. For $Ho_2Fe_{17}H_4$, the temperature dependence of the elastic intensity appears to be significant even below 120 K. This suggests that the H jump motion in $Ho_2Fe_{17}H_4$ is considerably faster than that in $Y_2Fe_{17}H_{4.2}$, at least at low temperatures. Such a conclusion is supported by the other data (to be discussed below). On the basis of the fixed-window scans, QENS spectra were measured on HFBS at 140 K and 160 K for $Y_2Fe_{17}H_{4.2}$ and at 100 K and 120 K for $Ho_2Fe_{17}H_4$. Additional measurements at $T = 4.2$ K were used to determine the instrumental resolution functions for HFBS. The QENS spectra measured on HFBS are also reasonably described by Eq. (1) convoluted with the corresponding resolution function.

The analysis based on Eq. (1) yields the values of Γ and $A_0(Q)$ for each spectrum. Since the half-width of the quasielastic component is found to be nearly Q-independent, at the next stage of the analysis, the values of Γ were fixed to their average values at a given temperature, and the Q dependence of A_0 was derived from the fits

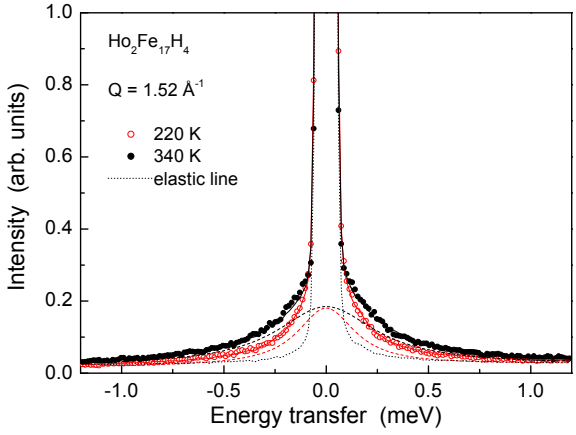

Fig. 4. The QENS spectra for $Ho_2Fe_{17}H_4$ measured on DCS at $Q = 1.52$ Å^{-1} at two temperatures: 220 K (red symbols) and 340 K (black symbols). The full curves show the fits of the two-component model (Eq. (1)) to the data. The dotted curve represents the elastic component (the spectrometer resolution function), and the dashed curves show the Lorentzian quasielastic components. (For interpretation of the references to colour in this figure legend, the reader is referred to the web version of this article.)

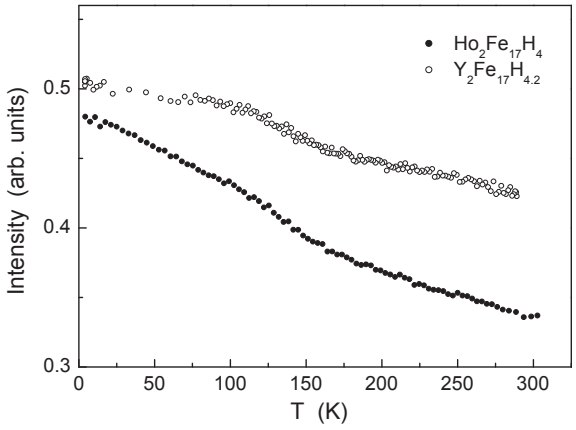

Fig. 5. The temperature dependences of the elastic scattering intensities for $Ho_2Fe_{17}H_4$ and $Y_2Fe_{17}H_{4.2}$ measured over the Q range of 0.87–1.68 Å^{-1} using the fixed-window operation mode of HFBS.

of the two-component model (Eq. (1)) with the fixed Γ. We shall start with a discussion of the Q dependence of the elastic incoherent structure factor (EISF) A_0, which is related to the geometry of localized H motion [33,34]; the temperature dependence of Γ will be discussed later. In order to obtain the EISF for the hydrogen sublattice, the A_0 values resulting from the fits were corrected for the small Q-independent elastic contribution of the host-metal lattice. Figs. 6 and 7 show the Q dependences of the EISF for the H sublattice in $Ho_2Fe_{17}H_4$ and $Y_2Fe_{17}H_{4.2}$, respectively, at two temperatures. For the measurements at other temperatures, the Q dependences of the EISF have similar shapes. However, as can be seen from Figs. 6 and 7, for both compounds the measured EISF is temperature dependent, decreasing with increasing T. This feature is common to many intermetallic hydrides, including Laves phases [36–39], $Pr_2Fe_{17}H_x$ [17,18], and $Ce_2Fe_{17}H_5$ [19]; it can be accounted for in terms of a temperature-dependent fraction of H atoms participating in the localized jump motion on the time scale of the QENS measurements [36,38]. First, we have to verify whether the observed shape of Q dependence of the EISF in $Ho_2Fe_{17}H_4$ and $Y_2Fe_{17}H_4$ is consistent with H jump motion over the hexagons formed by the tetrahedral (12i) sites. Since the distance between the nearest-neighbor tetrahedral 12i sites in $Ho_2Fe_{17}H_4$ ($r_{ii} = 1.17$ Å for $Ho_2Fe_{17}D_{3.6}$ [6]) is considerably shorter than the distances both between the nearest-neighbor 6h and 12i sites ($r_{hi} = 2.53$ Å [6]) and between the nearest-neighbor octahedral 6h sites ($r_{hh} > 4$ Å), it is reasonable to assume that H atoms at the octahedral 6h sites (3 H atoms per formula unit of Ho_2Fe_{17}) are immobile on the time scale of our measurements. Similar arguments are also applicable to $Y_2Fe_{17}H_{4.2}$, where the intersite distances are very close to those in $Ho_2Fe_{17}H_4$. Assuming further that only a fraction p of H atoms in tetrahedral 12i sites participate in the fast localized motion, the orientationally averaged EISF for the model of jumps between six equidistant sites on a circle of radius r [33] can be written in the form

$$A_0(Q) = 1 - \frac{(x-3)p}{x} + \frac{(x-3)p}{6x}\left[1 + 2j_0(Qr) + 2j_0\left(Qr\sqrt{3}\right) + j_0(2Qr)\right], \quad (2)$$

where x is the hydrogen content (per formula unit) and $j_0(y)$ is the spherical Bessel function of zeroth order, $j_0(y) = \sin y/y$. Solid lines in Fig. 6 show the fits of this six-site model (with the value of r fixed to $r_{ii} = 1.17$ Å) to the EISF data for $Ho_2Fe_{17}H_4$. The only fit parameter is the temperature-dependent fraction p which is responsible for the range of the EISF variation. It can be seen from Fig. 6 that the observed Q dependence of the EISF is consistent with the model of H jump motion over the hexagons formed by the tetrahedral 12i sites. A similar approach with the same fixed value of r was also used for the description of the EISF data for $Y_2Fe_{17}H_{4.2}$; the results of the fits at two temperatures are shown by solid lines in Fig. 7.

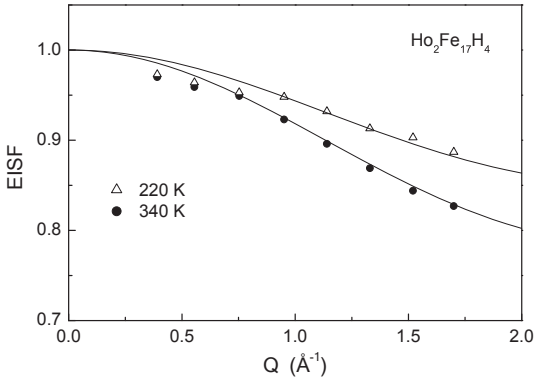

Fig. 6. The elastic incoherent structure factor for the hydrogen sublattice in $Ho_2Fe_{17}H_4$ as a function of Q at $T = 220$ K and 340 K. The curves show the fits of the six-site model (Eq.(2)) with fixed $r = 1.17$ Å to the data.

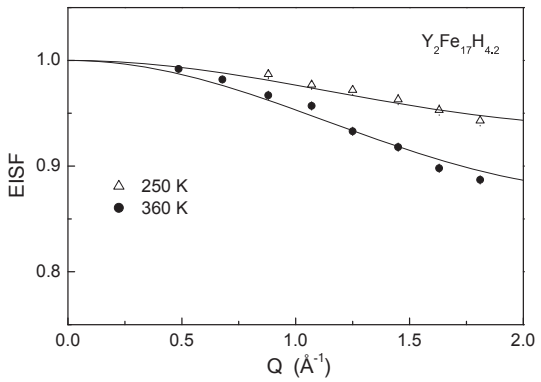

Fig. 7. The elastic incoherent structure factor for the hydrogen sublattice in $Y_2Fe_{17}H_{4.2}$ as a function of Q at $T = 250$ K and 360 K. The curves show the fits of the six-site model (Eq. (2)) with fixed $r = 1.17$ Å to the data.

The temperature dependences of the fraction p resulting from the fits of Eq. (2) to the DCS data for $Ho_2Fe_{17}H_4$ and $Y_2Fe_{17}H_{4.2}$ are shown in Fig. 8. As can be seen from this figure, the value of p for $Ho_2Fe_{17}H_4$ increases with increasing T, approaching 1 at the highest temperature of our measurements. The shape of $p(T)$ for $Y_2Fe_{17}H_{4.2}$ appears to be similar; however, the values of p are considerably lower than those for $Ho_2Fe_{17}H_4$ over the entire temperature range studied. It should be noted that for rhombohedral $Pr_2Fe_{17}H_x$ [17,18] and $Ce_2Fe_{17}H_5$ [19], qualitatively similar $p(T)$ behavior was observed. The increase of p with increasing temperature was also reported for localized H motion in α-ScH_x [40], α-$LaNi_5H_x$ [41], and Laves-phase hydrides [36–39]; in these cases, the presence of the immobile proton fraction $1 - p$ was attributed to H–H interactions giving rise to a formation of some ordered H configurations, which are progressively destroyed at higher temperatures due to thermal fluctuations. For Laves-phase hydrides, this interpretation is supported by the observed decrease of p with increasing hydrogen concentration [42]. However, the applicability of such an interpretation to $R_2Fe_{17}H_x$ compounds is questionable. Indeed, for $x = 5$, each hexagon formed by the tetrahedral sites in these compounds is occupied by two H atoms. Because of the 'blocking' effect [13], two hydrogen atoms can only occupy the opposite vertices of each

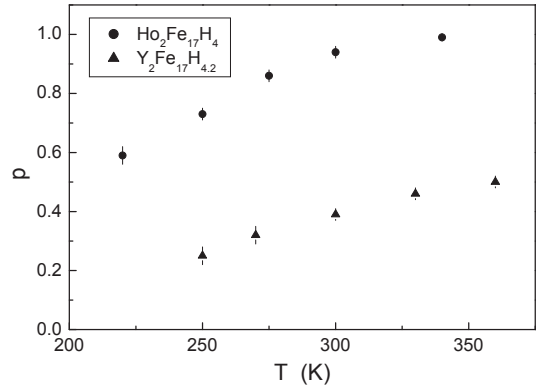

Fig. 8. The temperature dependences of the fractions of H atoms in 12i sites participating in the fast localized motion in $Ho_2Fe_{17}H_4$ and $Y_2Fe_{17}H_{4.2}$.

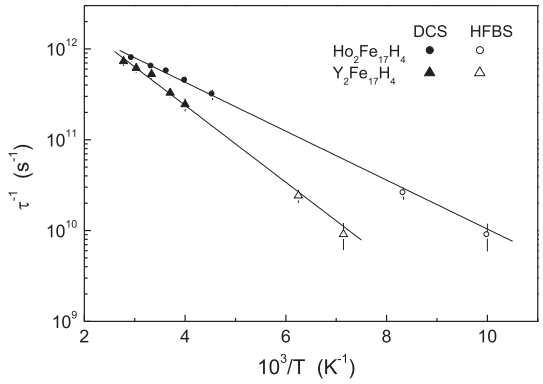

Fig. 9. The hydrogen jump rates as functions of the inverse temperature for $Ho_2Fe_{17}H_4$ and $Y_2Fe_{17}H_{4.2}$. The lines show the Arrhenius fits to the data obtained on both DCS and HFBS.

hexagon [8]. In this configuration, two H atoms are expected to block each other's *random* jumps over the hexagon. Nevertheless, in both $Pr_2Fe_{17}H_5$ [17] and $Ce_2Fe_{17}H_5$ [19], the values of the mobile fraction p were found to be close to 1 at high temperatures. This suggests a correlated motion of two H atoms on the same hexagon, as if they formed a bound pair. Furthermore, in the case of $Pr_2Fe_{17}H_x$, it was found [18] that the values of p for compounds with $x = 5$ and 4 are nearly the same. Thus, removing one-half of H atoms from the tetrahedral interstitial sites does not lead to any significant increase of the fraction of mobile hydrogen atoms. This result suggests that the immobilization of some hydrogen atoms at the tetrahedral sites may originate from defects in the host-metal lattice, rather than from H–H interactions. For hexagonal $Ho_2Fe_{17}H_4$ and $Y_2Fe_{17}H_{4.2}$, both the lattice parameters and H concentrations are close to each other, whereas the values of p in these compounds differ significantly (Fig. 8). Therefore, it is also reasonable to assume that defects in the host-metal lattice play the main role in the partial H immobilization in these compounds. Indeed, host-lattice distortions may also distort the hexagons formed by the tetrahedral sites, making some of them unsuitable for fast localized hydrogen motion. It should be noted that some hexagonal R_2Fe_{17} compounds are known to have a partially disordered crystal structure with an excess of Fe atoms with respect to the ideal 2:17 ratio [2,43]. Such excess Fe atoms may be responsible for partial H immobilization.

We now turn to a discussion of the temperature dependence of the jump rate, τ^{-1}, of the localized H motion. This rate is proportional to the half-width Γ of the quasielastic component in QENS spectra; however, the exact relation between Γ and τ^{-1} depends on the actual model of localized motion. A rigorous description in terms of the six-site model [33] predicts that the quasielastic component of the QENS spectrum is a sum of three Lorentzian lines with the half-widths $0.5\hbar\tau^{-1}$, $1.5\hbar\tau^{-1}$, and $2\hbar\tau^{-1}$, and Q-dependent amplitudes. It should be noted that at $Qr < 2$ (which corresponds to our experimental Q range) this sum is strongly dominated by the Lorentzian with the half-width of $0.5\hbar\tau^{-1}$ [33]. Because of the limited experimental accuracy, in this Q range, it is practically impossible to distinguish between the three-component quasielastic line and the single Lorentzian with the Q independent width. Therefore, we have adopted a simplified description based on the single Lorentzian with $\Gamma = 0.5\hbar\tau^{-1}$. The resulting temperature dependences of τ^{-1} for $Ho_2Fe_{17}H_4$ and $Y_2Fe_{17}H_{4.2}$ are shown in Fig. 9. It can be seen that a combination of the time-of-flight and backscattering QENS data allows us to probe the changes in the H jump rate over a range of nearly two orders of magnitude. For both compounds, the temperature dependences of τ^{-1} are satisfactorily described by the Arrhenius law,

$$\tau^{-1} = \tau_0^{-1}\exp(-E_a/k_BT), \quad (3)$$

where E_a is the activation energy for the localized H motion. The solid lines in Fig. 9 show the Arrhenius fits to the $\tau^{-1}(T)$ data; the corresponding fit parameters are $\tau_0^{-1} = 5.1\ (9) \times 10^{12}\ s^{-1}$ and $E_a = 54\ (4)$ meV for $Ho_2Fe_{17}H_4$, and $\tau_0^{-1} = 1.2\ (3) \times 10^{13}\ s^{-1}$ and $E_a = 84\ (7)$ meV for $Y_2Fe_{17}H_{4.2}$. At low temperatures, the hydrogen jump motion in $Ho_2Fe_{17}H_4$ is considerably faster than that in $Y_2Fe_{17}H_{4.2}$; this is consistent with the fixed-window scan data discussed above. It should be noted that previous Mössbauer studies of $Ho_2Fe_{17}D_{3.8}$ [44] have not revealed any effects that could be ascribed to slowing down of deuterium motion on the Mössbauer time scale of 100 ns at low temperatures.

Activation energies and H jump rates at 300 K for different R_2Fe_{17} hydrides are compared in Table 1. It can be seen that $Ho_2Fe_{17}H_4$ exhibits the lowest activation energy and the fastest H jump motion among all R_2Fe_{17} hydrides studied so far. Furthermore, the localized hydrogen motion in the hexagonal Th_2Ni_{17}-type hydrides appears to be faster than in the rhombohedral Th_2Zn_{17}-type hydrides. In contrast to the case of Laves-phase hydrides [38], we have not found any clear correlation between the H jump rates and the nearest-neighbor distances within the hexagons formed by the tetrahedral sites in R_2Fe_{17} hydrides. For example, the change in this nearest-neighbor distance from 1.08 Å for $Ce_2Fe_{17}H_5$ [19] to 1.17 Å for $Ho_2Fe_{17}H_4$ does not lead to the expected decrease in the H jump rate in $Ho_2Fe_{17}H_4$. It should be noted, however, that for Laves-phase hydrides, the range of the hexagon size variations is much wider than for R_2Fe_{17} hydrides.

Table 1
Activation energies for hydrogen jump motion and H jump rates at 300 K derived from QENS measurements in R_2Fe_{17} hydrides.

Compound	Structure type	E_a, meV	τ^{-1} (300 K), s^{-1}	Ref.
$Pr_2Fe_{17}H_5$	Th_2Zn_{17} (rhomb.)	140 (10)	7.4×10^{10}	[17]
$Ce_2Fe_{17}H_5$	Th_2Zn_{17} (rhomb.)	103 (3)	2.6×10^{11}	[19]
$Y_2Fe_{17}H_{4.2}$	Th_2Ni_{17} (hex.)	84 (7)	4.6×10^{11}	this work
$Ho_2Fe_{17}H_4$	Th_2Ni_{17} (hex.)	54 (4)	6.4×10^{11}	this work

4. Conclusions

The results of our neutron vibrational spectroscopy measurements for the isomorphous hexagonal $Ho_2Fe_{17}H_4$ and $Y_2Fe_{17}H_{4.2}$ are consistent with the locations of hydrogen atoms in both the octahedral 6*h* and the tetrahedral 12*i* sites in these compounds. The analysis of our quasielastic neutron scattering data has shown that H atoms occupying the tetrahedral sites in both compounds participate in the fast localized jump motion over the hexagons formed by these sites. At the frequency scale of $10^{10}\ s^{-1}$ this motion is observable even below 150 K. However, the fraction of mobile H atoms is found to decrease with decreasing temperature. The temperature dependence of the hydrogen jump rate τ^{-1} is well described by the Arrhenius law over wide T ranges (100–340 K for $Ho_2Fe_{17}H_4$ and 140–360 K for $Y_2Fe_{17}H_{4.2}$); the corresponding activation energies are 54 (4) meV and 84 (7) meV, respectively. It should be noted that these activation energy values are considerably lower than those found for H motion in the rhombohedral compounds $Pr_2Fe_{17}H_5$ [17] and $Ce_2Fe_{17}H_5$ [19]. For $Ho_2Fe_{17}H_4$, the localized hydrogen jump motion is found to be the fastest among all R_2Fe_{17} hydrides studied so far. At room temperature, the H jump rate in $Ho_2Fe_{17}H_4$ derived from our QENS data reaches $6.4 \times 10^{11}\ s^{-1}$.

Acknowledgments

This work was performed within the assignment of the Russian Federal Agency of Scientific Organizations (program "Spin" No. 012014633). The authors acknowledge support from the Ural Branch of the Russian Academy of Sciences under grant No. 15-9-2-9. AVS gratefully acknowledges financial support from the NIST Center for Neutron Research. This work utilized facilities supported in part by the National Science Foundation under Agreement No. DMR-0944772.

References

[1] K.H.J. Buschow, J. Less-Common Met. 11 (1966) 200–206.
[2] D. Givord, R. Lemaire, J.M. Moreau, E. Roudaut, J. Less-Common Met. 29 (1972) 361–369.
[3] O. Prokhnenko, J. Kamarad, K. Prokes, Z. Arnold, A.V. Andreev, Phys. Rev. Lett. 94 (2005) 107201.
[4] E.A. Tereshina, A.V. Andreev, J. Kamarad, O. Isnard, K. Watanabe, J. Phys. Condens. Matter 23 (2011) 216004.
[5] Y. Skourski, M.D. Kuz'min, K.P. Skokov, A.V. Andreev, J. Wosnitza, Phys. Rev. B 83 (2011), 214420.
[6] O. Isnard, S. Miraglia, J.L. Soubeyroux, D. Fruchart, A. Stergiou, J. Less-Common Met. 162 (1990) 273–284.
[7] O. Isnard, S. Miraglia, D. Fruchart, J. Deportes, J. Magn. Magn. Mater. 103 (1992) 157–164.
[8] O. Isnard, S. Miraglia, J.L. Soubeyroux, D. Fruchart, P. L'Héritier, J. Magn. Magn. Mater. 137 (1994) 151–156.
[9] O. Isnard, S. Miraglia, D. Fruchart, C. Giorgetti, S. Pizzini, E. Dartyge, G. Krill, J.P. Kappler, Phys. Rev. B 49 (1994) 15692–15701.
[10] H. Fujii, M. Akayama, K. Nakao, K. Tatami, J. Alloys Compd. 219 (1995) 10–15.
[11] O. Isnard, S. Miraglia, D. Fruchart, E. Akiba, K. Nomura, J. Alloys Compd. 257 (1997) 150–155.
[12] D. Hautot, G.J. Long, F. Grandjean, O. Isnard, Phys. Rev. B 62 (2000) 11731–11741.
[13] A.C. Switendick, Z. Phys. Chem. N. F. 117 (1979) 89–112.
[14] O. Isnard, J.L. Soubeyroux, S. Miraglia, D. Fruchart, L.M. Garcia, J. Bartolome, Phys. B 180 (1992) 624–626.
[15] F. Cuevas, O. Isnard, B. Villeroy, Thermochim. Acta 561 (2013) 14–18.
[16] D. Hautot, G.J. Long, F. Grandjean, O. Isnard, S. Miraglia, J. Appl. Phys. 86 (1999) 2200–2207.
[17] E. Mamontov, T.J. Udovic, O. Isnard, J.J. Rush, Phys. Rev. B 70 (2004) 214305.
[18] E. Mamontov, T.J. Udovic, J.J. Rush, O. Isnard, J. Alloys Compd. 422 (2006) 149–152.
[19] A.V. Skripov, N.V. Mushnikov, P.B. Terent'ev, V.S. Gaviko, T.J. Udovic, J.J. Rush, J. Phys. Condens. Matter 23 (2011), 405402.
[20] T.J. Udovic, C.M. Brown, J. Leão, P.C. Brand, R.D. Jiggets, R. Zeitoun, T.A. Pierce, I. Peral, J.R.D. Copley, Q. Huang, D.A. Neumann, R.J. Fields, Nucl. Instrum. Methods A 588 (2008) 406–413.
[21] J.R.D. Copley, J.C. Cook, Chem. Phys. 292 (2003) 477–485.
[22] A. Meyer, R.M. Dimeo, P.M. Gehring, D.A. Neumann, Rev. Sci. Instrum. 74 (2003) 2759–2777.
[23] D. Richter, R. Hempelmann, R.C. Bowman, in: L. Schlapbach (Ed.), Hydrogen in Intermetallic Compounds II, Springer, Berlin, 1992, p. 97.
[24] D.K. Ross, in: H. Wipf (Ed.), Hydrogen in Metals III, Springer, Berlin, 1997, pp. 153–214.
[25] T.J. Udovic, W. Zhou, H. Wu, C.M. Brown, J.J. Rush, T. Yildirim, E. Mamontov, O. Isnard, J. Alloys Compd. 446–447 (2007) 504–507.
[26] J.C. Slater, J. Chem. Phys. 41 (1964) 3199–3204.
[27] O. Isnard, S. Miraglia, J.L. Soubeyroux, D. Fruchart, Solid State Commun. 81 (1992) 13–19.
[28] H. Müller, P. Knappe, O. Greis, Z. Phys. Chem. N. F. 114 (1979) 45–50.
[29] T.J. Udovic, J.J. Rush, Q. Huang, I.S. Anderson, J. Alloys Compd. 253–254 (1997) 241–247.
[30] T.J. Udovic, Q. Huang, J.J. Rush, J. Alloys Compd. 356–357 (2003) 241–247.
[31] V.E. Antonov, K. Cornell, V.K. Fedotov, A.I. Kolesnikov, E.G. Ponyatovsky, V.I. Shiryaev, H. Wipf, J. Alloys Compd. 264 (1998) 214–222.
[32] K. Cornell, H. Wipf, V.E. Antonov, T.E. Antonova, A.I. Kolesnikov, E.G. Ponyatovsky, B. Dorner, Pol. J. Chem. 71 (1997) 1792–1796.
[33] M. Bée, Quasielastic Neutron Scattering, Hilger, Bristol, 1988.
[34] R. Hempelmann, Quasielastic Neutron Scattering and Solid State Diffusion, Clarendon Oxford, 2000.
[35] T.J. Udovic, N. Verdal, J.J. Rush, D.J. De Vries, M.R. Hartman, J.J. Vajo, A.F. Gross, A.V. Skripov, J. Alloys Compd. 580 (2013) S47–S50.
[36] A.V. Skripov, J.C. Cook, D.S. Sibirtsev, C. Karmonik, R. Hempelmann, J. Phys. Condens. Matter 10 (1998) 1787–1801.
[37] A.V. Skripov, J.C. Cook, T.J. Udovic, V.N. Kozhanov, Phys. Rev. B 62 (2000) 14099–14104.
[38] A.V. Skripov, Defect Diffus. Forum 224–225 (2003) 75–92.
[39] A.V. Skripov, T.J. Udovic, J.J. Rush, Phys. Rev. B 76 (2007), 104305.
[40] N.F. Berk, J.J. Rush, T.J. Udovic, I.S. Anderson, J. Less-Common Met. 172–174 (1991) 496–508.
[41] C. Schönfeld, R. Hempelmann, D. Richter, T. Springer, A.J. Dianoux, J.J. Rush, T.J. Udovic, S.M. Bennington, Phys. Rev. B 50 (1994) 853–865.
[42] A.V. Skripov, T.J. Udovic, J.J. Rush, M.A. Uimin, J. Phys. Condens. Matter 23 (2011) 065402.
[43] O. Isnard, D. Hautot, G.J. Long, F. Grandjean, J. Appl. Phys. 88 (2000) 2750–2759.
[44] G.J. Long, O. Isnard, F. Grandjean, J. Appl. Phys. 91 (2002) 1423–1430.